Postprint of: Dettlaff A., Skowierzak G., Macewicz Ł., Sobaszek M., Karczewski J., Sawczak M., Ryl J., Ossowski T., Bogdanowicz R., Electrochemical Stability of Few-Layered Phosphorene Flakes on Boron-Doped Diamond: A Wide Potential Range of Studies in Aqueous Solutions, The Journal of Physical Chemistry C, Vol 123, iss 33 (2019), pp. 20233–20240 DOI: 10.1021/acs.jpcc.9b03028

# Electrochemical Stability of Few-Layered Phosphorene Flakes on Boron-Doped Diamond: A Wide Potential Range of Studies in Aqueous Solutions

**ABSTRACT:** Two-dimensional phosphorene has attracted great interest since its discovery as a result of its extraordinary properties. Two-dimensional single crystals of phosphorene can be useful for electrochemical (EC) sensing applications due to their enhanced surface-to-volume ratio. We proposed to investigate the electrochemical performance of phosphorene deposited directly on boron-doped diamond (BDD) electrodes. Noncovalent interaction of phosphorene with BDD was achieved due to van der Waals interactions. This extends the potential range of EC studies in aqueous solutions due to the extraordinary wide range of the BDD potential window (−2 to 2.5 V vs Ag|AgCl|3M KCl). Cyclic voltammetry studies demonstrated irreversible electrochemical oxidation of the phosphorene, with peaks observed at different potentials depending on the sonication power during the liquid exfoliation of black phosphorus (BP). This indicated the formation of polyphosphoric quasi-oxide layers with undefined oxidation states of phosphorus. Electrochemical impedance spectroscopy showed the second time constant for high-power sonicated BP, which was attributed to $P_xO_y(OH)_z$ formation. The subsequent film was responsible for limiting the charge transfer rate. The BDD enabled the EC behavior of phosphorene to be studied at high anodic potentials.

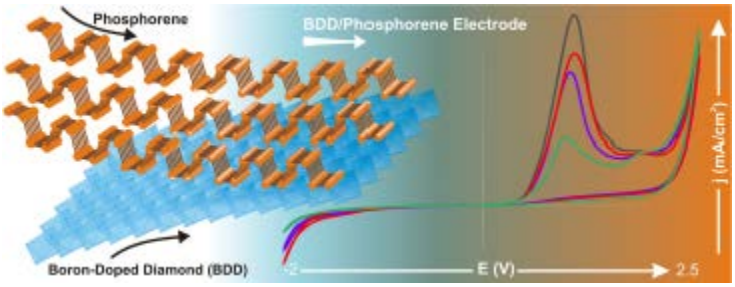


## INTRODUCTION

In recent years, two-dimensional (2D) few-layered materials have gained increasing attention due to their fascinating optical, electrochemical (EC), and mechanical properties in comparison to their multilayered bulk counterparts.1,2 This group forms part of the widely studied 2D nanomaterials, such as graphene, molybdenum disulfide, and phosphorene, the latter having attracted much research interest since its discovery in 2014.3,4 Phosphorene exhibits many desirable properties like high anisotropy,5 high carrier mobility,6 good biocompatibility,7,8 and high mechanical flexibility.9 However, one of its most unusual properties is the direct and tunable band gap.10 Its value depends on the number of layers and is equal to 0.3 eV for bulk black phosphorus (BP) and approx. 1.3 eV for a phosphorene monolayer.11 BP nanosheets can be fabricated via liquid-phase exfoliation of BP in N-methyl-2-pyrrolidone (NMP) and other organic solvents, or by mechanical exfoliation of black phosphorus crystals.12,13 Liquid-phase exfoliation requires time-consuming sonication and reduces the lateral size of the synthesized BP flakes; however, the size of the fabricated flakes, as well as the concentration of the colloid, can be controlled by isolation procedures and tuning of the exfoliation conditions.14 Although black phosphorus is the most thermodynamically stable form of the main three phosphorus allotropes, it

degrades chemically under ambient conditions and special care must be taken during the exfoliation process.15,16

There are many studies that focus on finding the causes of BP surface deterioration, most of which are attributed to the negative simultaneous influence of light radiation, oxygen, and water on the thin BP layers, known as the aging process.17−19 Pristine phosphorus is hydrophobic, but the oxidation process changes the surface progressively to be hydrophilic. As a result a hydrogen bond is formed between surface-chemisorbed oxygen and hydrogen originating from water, leading to the P− P bond breaking. Likewise, there are many papers that include calculations for shifts in the energy for likely bonding configurations and the first-principles molecular dynamics proves that exposure of BP to oxygen may lead to various oxidation states of the material.20−22

In recent electrochemical studies on BP, the most commonly used substrate is glassy carbon.23,24 However, the measure-ments were conducted in the limited potential range (−0.9− 0.9 V vs Ag|AgCl). There are no studies that would fully exploit the electrochemical possibilities of BP flake behavior in aqueous electrolytes. Herein, we present the electrochemical testing of few-layered phosphorene flakes fabricated by liquid-phase exfoliation of black phosphorus drop-cast onto thin boron-doped diamond (BDD) films in an extraordinary range of potential window in aqueous electrolytes from −2 to 2.5 V vs Ag|AgCl|3M KCl.

## EXPERIMENTAL SECTION

**Chemicals.** All reagents were of analytical grade and used without further purification. The black phosphorus was purchased from Smart Elements. N-methyl-2-pyrrolidone was collected from Scharlau. Sodium sulfate (Stanlab) and potassium hexacyanoferrate(III) (Chempur) aqueous solutions involved the use of demineralized water. The synthesis gases (methane, hydrogen, and diborane) and other gases (nitrogen and argon) used for the BDD and BP preparation processes were purchased from Linde and were of the highest purity class.

**Boron-Doped Diamond Fabrication.** The BDD electrodes were deposited using the microwave plasma-assisted chemical vapor deposition (Seki Technotron AX5400 S, Japan) process on 10 × 10 $mm^2$ p-type silicon. The specific synthesis process details can be found elsewhere.25,26 Samples were doped using diborane ($B_2H_6$) dopant precursor; the [B]/[C] ratio was 10 000 ppm in the plasma, resulting in an acceptor concentration of 3 × 1021 $cm^{-3}$ after 6 h of deposition with approx. 2 μm film thickness. Next, a four-step pretreatment of the deposited electrode was applied to etch $sp^2$ phase impurities and obtain a H-terminated surface.27

**Liquid Exfoliation of Black Phosphorus.** Precrushed BP (30 mg) was added to the anhydrous N-methyl-2-pyrrolidone (5 mL) under an argon atmosphere. Next, the sample was moved into a hermetic vessel to the measurement site, consisting of a horn probe ultrasonicator (Bandelin Sonopuls HD2200, 20 kHz, 50/50 time amplitude) and a bath sonicator (Polsonic 3, 160 W, 40 kHz). The process of exfoliation was carried out in ice bath under a stream of nitrogen. The sonication power of the ultrasonicator was gradually increased to either 20, 40, or 100 W. The sonication-aided exfoliation process took 75 min, involving 5 min for increasing the sonication power, 60 min for the main process, and 10 min for cooling the probe (no sonication).

The prepared slurry (30 μL) was drop-cast on boron-doped diamond wafers. The last step in the preparation of the electrodes for measurement was electrode drying with the applied NMP/BP suspension in a vacuum oven for solvent evaporation (Figure 1). Depending on the ultrasonication power, three sets of few-layered phosphorene samples were obtained: BDD/BP-20W, BDD/BP-40W, and BDD/BP-100W.

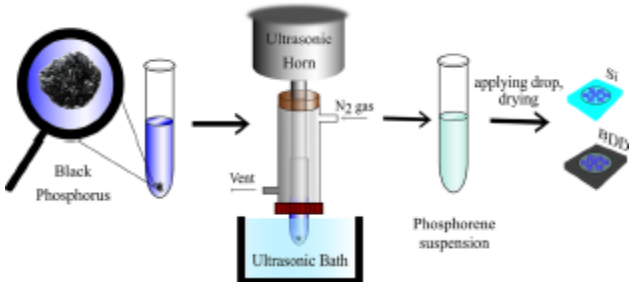


*Figure 1. Few-layered phosphorene preparation scheme.*

**Characterization Techniques.** The Raman spectra were recorded using a micro-Raman spectrometer (InVia, Renishaw, U.K.). The excitation wavelength was 514 nm (Ar ion laser), and the wavenumber was in the range of 300−600 $cm^{-1}$. The morphology of the few-layered phosphorene electrode layers was characterized by a scanning electron microscope (SEM)(FEI Quanta FEG 250). A 10 kV beam accelerating voltage was used with a secondary electron Everhart−Thornley detector working in high vacuum mode pressure of $10^{-4}$ Pa. The UV absorption of the black phosphorus layers dispersed in NMP was measured by a vis−NIR spectrometer (UV-900, Metash, China).

The electrochemical properties of few-layered phosphorene were investigated by cyclic voltammetry (CV) and electrochemical impedance spectroscopy (EIS) using a potentiostat− galvanostat (VMP-300, Bio-Logic, France) driven by EC-Lab software. All electrochemical tests were carried out in a three-electrode electrochemical cell under an argon atmosphere. The BDD electrode with few-layered phosphorene was used as the working electrode. The Ag|AgCl|3.0 M KCl electrode and Pt wire served as the reference electrode and the counter-electrode, respectively. The diameter of the round working electrode area (wetted by the electrolyte) was 5 mm. The CV measurements were conducted in contact with an aqueous, deoxygenated 0.5 mol $dm^{-3}$ $Na_2SO_4$ solution and measured for chosen sweep rates in the 10−100 mV $s^{-1}$ range. The potential window was from −2.0 to 2.5 V vs Ag|AgCl|3.0 M KCl. Cyclic voltammetry was also carried out in 5 mM $Fe(CN)_6^{3-/4-}$ in a 0.5 mol $dm^{-3}$ $Na_2SO_4$ solution at 100 mV $s^{-1}$. Electrochemical impedance spectroscopy was performed in a wide frequency range from 0.1 Hz to 100 kHz in a 0.5 mol $dm^{-3}$ $Na_2SO_4$ solution. Spectra were recorded at the rest potential with a peak-to-peak amplitude of 10 mV and 6 points per frequency decade. Prior to the measurements, the working electrode was initially conditioned.

## RESULTS AND DISCUSSION

### Characterization of Structure and Morphology.

Optical absorption measurements can be performed to yield quantitative information about BP thickness, as widely reported by other authors.28−30 We decided to use vis−NIR spectroscopy as a method to estimate the number of layers in the prepared BP flakes. The spectroscopic test was conducted by diluting the primary BP solution in NMP. Absorbance spectra were obtained for solutions immediately after the centrifugation process. The vis−NIR spectrum of the BDD/BP-20W electrode (Figure 2a) showed that the sample exhibited optical activity across the whole analyzed range, with absorbance increasing toward the lower wavelengths, as previously reported.31 The vis−NIR absorption spectrum shows an electronic band-to-band transition at a high energy of 2.48 eV (480 nm), revealing a structure typical of four-layer dominated systems, as reported by Woomer et al.31

The next step was the surface morphology analysis. The scanning electron microscopy results (Figure 2b) show that the drop-casting process was performed successfully, with a strongly compacted nanostructure constructed from nano-sheets of various sizes. It can also be observed that the phosphorene film consists of multiple layers that correspond to the results obtained from vis−NIR spectroscopy. The thickness of the BDD and BP layers was determined by the cross section of the BDD/BP-20W electrode (Figure S1a) and was ca. 4.2 μm. Additionally, Figure S1b shows a view from the top of a pure BDD electrode.

The Raman spectra (Figure 2c), in turn, revealed noticeable maxima near 363, 439, and 467 $cm^{-1}$, corresponding to $A_g^1$, $B_{2g}$,and $A_g^2$ modes, respectively. These vibrations we attributed to few-layered phosphorene modes.32,33 The type of crystalline site vibrations corresponding to each mode is schematically presented in Figure 2d. As reported by other authors,34,35 the $B_{2g}$ mode was not observed for single-layer phosphorene and appeared when there were more than three layers. The relative band intensities in the Raman spectra recorded for the exfoliated material were nearly identical to those observed for the bulk material; however, a slight blue shift as well as narrowing of the Raman bands could be observed in the case of the thin-layer sample. The numerical simulation of the black phosphorene atomic vibrational modes showed a correlation between the vibration frequency of each mode and material strain.36 Depending on the compressing or stretching nature of the strain in the armchair and zigzag directions (Figure 2d), a blue or red shift could be observed in the Raman spectra. However, the correlation factors of the frequency shift and stress were individual for each vibrational mode. According to the above numerical predictions, the blue shift observed for the exfoliated material could be assigned to a weak (less than 1%) compressing strain of the phosphorene atomic site. The stress was associated

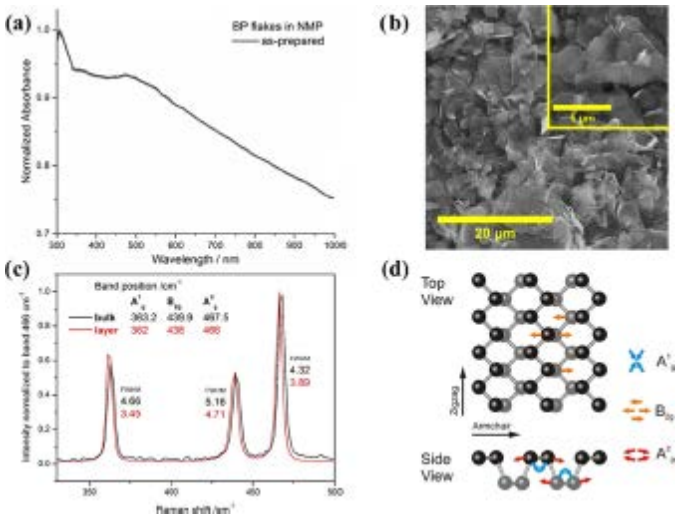


*Figure 2. Structural and optical characterizations of the BDD/BP-20W flakes: (a) vis−NIR spectrum, (b) SEM images at a magnification of 2500× and inset at 10 000×, (c) Raman spectra of bulk and exfoliated BP, and (d) atomic structure of phosphorene.*

with the bending forces acting on the individual phosphorene flakes in the thin film deposited on the substrate, which was confirmed by SEM inspection of the sample surface (Figure 2b).

**Electrochemical Studies.** The cyclic voltammetry and electrochemical impedance spectroscopy techniques were applied to determine the differences in the electrochemical activity of materials fabricated under different conditions. Figure 3 shows the cyclic voltammetry curves as a function of the scan rate of the BDD/BP-20W, BDD/BP-40W, and BDD/BP-100W layers.

The CV results demonstrate that the material underwent an irreversible oxidation process in the applied polarization range, a conclusion based on the absence of reduction current peaks. Furthermore, the anodic peak maximum shifted in potential with the sweep rate to more positive potentials (from 0.55 to 0.75 V), which could indicate the complex mechanism of the oxidation process. This may indicate that the final products of the reaction affect the BDD/BP surface.

According to the literature, the peak observed at ∼0.6 V (vs Ag|AgCl|3M KCl) corresponds to the electrochemical oxidation of elemental phosphorus $P^0$ to the fifth oxidation state, forming $PO_4^{3-}$ ions. Once oxidation occurs, water dissolves the oxides into a solution, forming phosphoric acid (eq 1).19,23,24,37

$$P + 4H_2O \rightarrow H_3PO_4 + 5H^+ + 5e^- \quad (1)$$

Contrary to the BDD/BP-20W layer, in which water reacts with pristine phosphorus, the other layers underwent different oxidation mechanisms. According to the literature, phosphorus may oxidize to form different chemical bonds with oxygen. These oxides can be generally described as $P_xO_y(OH)_z$.20 The difference among BDD/BP-20W, BDD/BP-40W, and BDD/BP-100W may be caused by the synthesis conditions. The higher the power of the ultrasonicator used to prepare the BDD/BP sample, the more the oxidation potential shifts toward more positive values. Thus, much more energy (overvoltage E) was necessary to oxidize the phosphorus oxide made on BDD/BP-40W and BDD/BP-100W electrodes contrary to that on BDD/BP-20W (Figure 3d). It is known that atomically thin 2D nanomaterials show high sensitivity to the synthesis conditions, which strongly influence the material structure due to their high surface area and unsaturated valences.38,39 We assumed that by increasing the power in the sonication process, the number of imperfections on the phosphorene lattice would increase. The density functional theory (DFT) simulations suggested that the defects present in the puckered phosphorene structure could greatly promote $O_2$ adsorption (the oxidizing rate is 5000 faster at a defect site comparing to that at a perfect BP site).38 As a result, on BDD/BP-40W and BDD/BP-100W, polyphosphoric quasi-oxide layers with undefined oxidation states of phosphorus were formed. According to calculations based on the framework of DFT, the oxidation of phosphorene can lead to the formation of native phosphorus oxides and suboxides, which may act as a passivation layer.20,22 In addition, the phosphorus−oxygen bond may be dangling (P=O) or

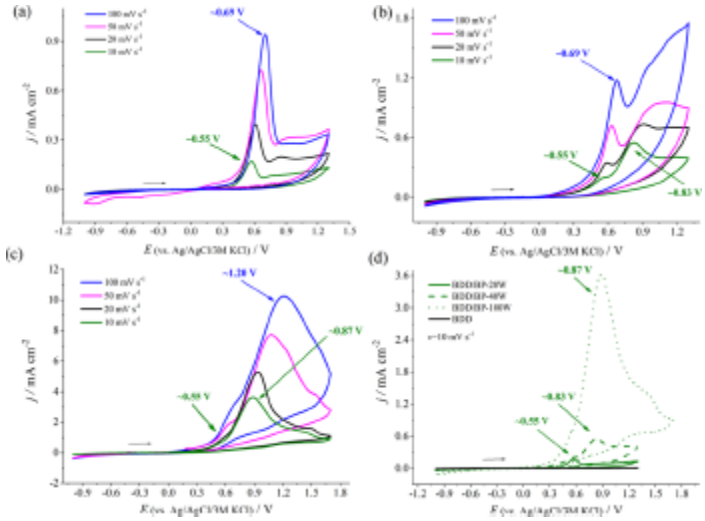

*Figure 3. Cyclic voltammetry results of (a) BDD/BP-20W, (b) BDD/BP-40W, and (c) BDD/BP-100W measured at various scan rates in 0.5 M Na2SO4; (d) comparison of CV curves at 10 mV s−1.*

bridging, when the oxygen bonds between two P atoms. It is worth mentioning that most P−O structures are insulators with a wide band gap, contrary to the pristine BP that exhibits semiconducting proper-ties.20,22,40 Figure 3b,c shows an evident extraction of the peak at approx. 0.83−0.87 and approx. 1.20 V at the expense of the peak at ∼0.55 V vs Ag|AgCl|3.0 M KCl, which may correspond to another oxidation states of $P_xO_y(OH)_z$ polymorphs.

For better understanding of this phenomenon, the BDD/BP-100W electrodes were investigated over a wide potential range, from −2.0 to 2.5 V vs Ag|AgCl|3M KCl in the aqueous electrolyte at 100 mV $s^{-1}$ (Figure 4). Figure 4b shows two scans of BDD/BP-20W. It should be noted that the peak at approx. 0.69 V disappeared in the second scan. It can be seen that the few-layered BP flakes were completely etched away. A similar electrochemical behavior is seen with overoxidized conducting polymers.41

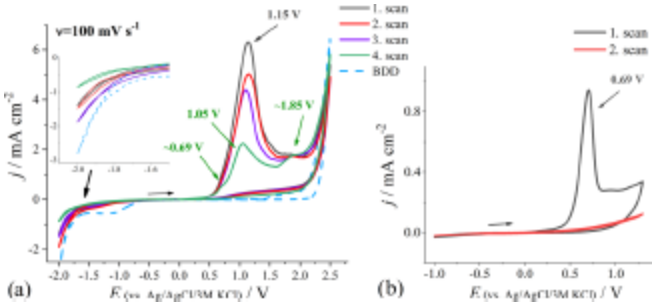

*Figure 4. Current density values as a cycle number function of (a) BDD/BP-100W and (b) BDD/BP-20W; v = 100 mV $s^{-1}$; outer electrolyte, 0.5 MNaSO4.*

On the other hand, the current density response of BDD/BP-100W observed at +1.15 V decayed more slowly (Figure 4a). Moreover, with the increase in cycle number, the area under this peak decreased, while the current density of the peak at +1.85 V increased simultaneously. A similar effect was visible for the peak associated with the oxidation of $P^0$ to $P^{+5}$ (+0.69 V), which may be related to the generation of hydrogen gas at potentials more negative than −1.8 V and oxidation of the bare phosphorus exposed after dissociation of the oxide layer. The loss of protection from the oxide barrier makes phosphorene susceptible to further oxidation. We assume that with each subsequent cathodic scan there was a reduction of $P_xO_y(OH)_z$ (first created during the forward scan), the broad peak at approx. −1.5 V. Next, the newly formed phosphorus oxide was further oxidized to another form of $P_xO_y(OH)_z$. These results were consistent with the previous investigation conducted by Pumera et al.17,23,24,42

They presented a study on the oxygen-induced aging of black phosphorus in protic solvents. The main products of the aging process determined by $^{31}P$ NMR spectroscopy were phosphorus oxoacids in various oxidation states: phosphorus monovalent $H_3PO_2$ ($P^{+1}$), trivalent $H_3PO_3$ ($P^{+3}$), tetravalent $H_4P_2O_6$ ($P^{+4}$), and pentavalent $H_3PO_4$

($P^{+5}$).17 The formation of acids, as products of BP degradation, can also be shown by pH measurement.43 We investigated the pH values of the compositions of the mixtures obtained after cyclic voltammetry analysis. The initial pH of 0.5 M $Na_2SO_4$ was 6.88 ± 0.06. After the electrochemical investigation, the pH value decreased to 4.81 ± 0.24, which confirmed that acidification occurred.

In the next step, the BDD/BP electrodes were investigated in the ferricyanide/ferrocyanide redox system to test the electron transfer activities (Figure 5). The bare BDD electrode response, prepared for the reference, is presented in Figure 5c. The peak-to-peak separation (ΔE) value of BDD was 180 mV.

As can be seen, the ΔE value was higher than the value of 59 mV, attributed to the electrochemically reversible redox couple. The increase in the peak-to-peak separation may be associated with the resistivity of the boron-doped diamond layer. On the other hand, the ΔE recorded for BDD/BP-20W was about 250 mV (Figure 5a). The peak-to-peak separation of BDD/BP-20W slightly decreases down to 220 mV once the electrochemical potential window is limited to ±0.5 V (not shown here). Moreover, the cathodic peak observed for the electrode studied in the narrower potential range is more pronounced. Reduction of potential range induces oxidation processes, a limitation of phosphorene layers. This result probably was related to the presence of sluggish electron transfer kinetics at the BP electrode surface and suggested the irreversibility of the system. It is worth mentioning that for BDD/BP-100W such redox activity was not observed, which may be associated with the presence of an oxygen barrier (Figure 5b).42

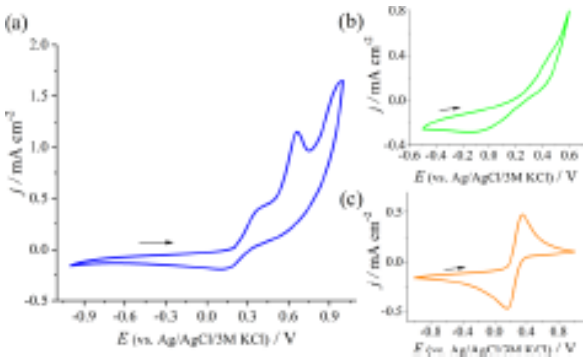


*Figure 5. Current density values as a function of the potential recorded at 100 mV $s^{-1}$ in contact with redox electrolyte 5 mM $K_3[Fe(CN)_6]$/0.5 M $Na_2SO_4$ recorded for (a) BDD/BP-20W and (b) BDD/BP-100W; (c) electrochemical response of the bare BDD electrode*

The Bode and Nyquist plot representations of the impedance spectra are shown in Figures 6 and S2, respectively. To perform further quantitative analyses of this data, the collected impedance data were approximated by an electric equivalent circuit (EEQC) using a ZSimpWin analyzer. The complex fitting of the impedance data (using the EEQC shown in the inset of Figure 6) is also presented in Figures 6 and 2S (solid lines). The fitting procedure gave normalized fitting errors, $\chi^2$, at the level of $10^{-4}$–$10^{-3}$. The values of each electrical parameter estimated using the aforementioned EEQC are shown in Table 1.

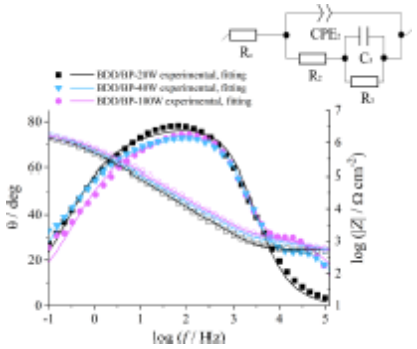


*Figure 6. Impedance data (points) and fitting (curve) of multilayered phosphorene (BDD/BP-20W, BDD/BP-40W, and BDD/BP-100W) recorded at the rest potential in contact with 0.5 M $Na_2SO_4$; reference electrode, Ag|AgCl. Inset: EEQC used for the fitting for all*

*Table 1. Selected Parameters Calculated from the Electrical Equivalent Circuit of the Impedance Spectra of BDD/BP Electrodes*

| | BDD/BP-20W | BDD/BP-40W | BDD/BP-100W |
|---|---|---|---|
| $Q_2/\mu\Omega^{-1}$ cm$^{-2}$ sn | 9.43 | 9.73 | 7.24 |
| $n_2$ | 0.72 | 0.70 | 0.71 |
| $R_2/\Omega$ cm$^2$ | $1.95 \times 10^{-5}$ | 44.9 | 70.1 |
| $C_3/\mu$Fcm$^{-2}$ | 2.02 | 1.11 | 0.83 |
| $R_3/k\Omega$ cm$^2$ | 71.0 | 100.3 | 78.3 |
| $\chi^2$ | $3.12 \times 10^{-3}$ | $8.84 \times 10^{-4}$ | $2.80 \times 10^{-3}$ |

The phase angle diagram in Figure 6 suggests the formation of two layers, which corresponds to the presence of two time constants. Thus, the EEQC was chosen assuming the existence of two partially overlapping time constants, represented by {$R_2$, $CPE_2$} and {$R_3$,$C_3$}, respectively. The first time constant, $\tau_2$,is related to the outer layer. The layer is visible, in particular, for BDD/BP-40W and BDD/BP-100W and may result from the formation of a $P_xO_y(OH)_z$ film on the surface of black phosphorus. The second time constant, $\tau_3$, may refer to the charge transfer process at the BDD/BP interface. The value of Re is determined by the electrolyte resistance. The charge transfer resistance changes significantly, together with a change in the synthesis conditions. The value of $R_2$ of BDD/BP-20W is close to zero, and the first time constant does not manifest itself on the Bode plots. It is worth noting that the time constant localized at the moderate-frequency range, $\tau_2$, generates additional charge transfer resistance, $R_2$, for BDD/BP-40W and BDD/BP-100W (44.9 and 70.1 Ω cm$^2$, respectively). However, the presence of $\tau_2$ does not affect the second (low-frequency) time constant $\tau_3$.Thus, $R_3$ oscillates in the range 70−100 kΩ cm$^2$.

The impedance of the constant phase element, $CPE_2$, reflects the distribution of reactivity caused by the interfacial heterogeneity interface.44−46 $CPE_2$ impedance is defined as $Z_{CPE2} = 1/Q_2(j\omega)^n$, where ω is the angular frequency [rad s$^{-1}$], j is the imaginary number, and $Q_2$ and n ($0 \leqslant\leq n \leqslant 1$) are the constant phase element parameters. The $CPE_2$ exponent, n, is sensitive to the texture of the interface and corresponds to the system inhomogeneity. Parameter n values did not change significantly and were about 0.7. This value indicated that the system was characterized by considerable heterogeneity. The capacitance $C_3$ decreased with the change in synthesis conditions from 2.02 to 0.825 μFcm$^{-2}$. The results suggested that it had double-layer capacitance.47

**CONCLUSIONS**

In this study, we have investigated for the first time the electrochemical performance and stability of a complex BDD/BP electrode. The phosphorene flakes were prepared from black phosphorous and N-methyl-2-pyrrolidone under ultra-sonic treatment and drop-cast on the BDD substrate. These electrodes were obtained and characterized at three different conditions, which were distinguished by the ultrasonicator power sets. Successful preparation of the few-layered phosphorene nanosheets was confirmed using electron microscopy and Raman spectroscopy, which showed that there were more than three layers. Furthermore, the vis−NIR spectrum revealed optical activity within the whole analyzed spectrum, with absorbance increasing toward lower wavelengths.

Cyclic voltammetry studies revealed the irreversible electro-chemical oxidation of the phosphorene when exposed to a 0.5 mol dm$^{-3}$ $Na_2SO_4$ solution. The reported peaks observed at different potentials for the BDD/BP-40W and BDD/BP-100W electrodes indicated the formation of polyphosphoric quasi-oxide layers with undefined oxidation states of phosphorus. The electrochemical impedance spectroscopy studies con-firmed the complex electrochemical response of the inves-tigated electrodes and the appearance of the second time constant for BDD/BP-40W and BDD/BP-100W samples, which was attributed to $P_xO_y(OH)_z$ formation. The following film was responsible for limiting the charge transfer rate.

**REFERENCES**

(1) Kou, L.; Chen, C.; Smith, S. C. Phosphorene: Fabrication, Properties, and Applications. J. Phys. Chem. Lett. 2015, 6, 2794−2805.
(2) Akhtar, M.; Anderson, G.; Zhao, R.; Alruqi, A.; Mroczkowska, J. E.; Sumanasekera, G.; Jasinski, J. B. Recent Advances in Synthesis, Properties, and Applications of Phosphorene. npj 2D Mater. Appl. 2017, 1, No. 5.

(3) Lu, W.; Nan, H.; Hong, J.; Chen, Y.; Zhu, C.; Liang, Z.; Ma, X.; Ni, Z.; Jin, C.; Zhang, Z. Plasma-Assisted Fabrication of Monolayer Phosphorene and Its Raman Characterization. Nano Res. 2014, 7, 853−859.
(4) Tran, V.; Soklaski, R.; Liang, Y.; Yang, L. Layer-Controlled Band Gap and Anisotropic Excitons in Few-Layer Black Phosphorus. Phys. Rev. B 2014, 89, No. 235319.
(5) Jain, A.; McGaughey, A. J. H. Strongly Anisotropic In-Plane Thermal Transport in Single-Layer Black Phosphorene. Sci. Rep. 2015, 5, No. 8501.
(6) Cai,Y.;Zhang, G.;Zhang,Y.ElectronicPropertiesof Phosphorene/Graphene and Phosphorene/Hexagonal Boron Nitride Heterostructures. J. Phys. Chem. C 2015, 119, 13929−13936.
(7) Pumera, M. Phosphorene and Black Phosphorus for Sensing and Biosensing. Trends Anal. Chem. 2017, 93,1−6.
(8) Ding, H.; Tang, Z.; Dong, Y. Synthesis of Black Phosphorus Quantum Dots Doped ZnO Nanoparticles and Its Electrogenerated Chemiluminescent Sensing Application. ECS J. Solid State Sci. Technol. 2018, 7, R135−R141.
(9) Wei, Q.; Peng, X. Superior Mechanical Flexibility of Phosphorene and Few-Layer Black Phosphorus. Appl. Phys. Lett. 2014, 104, No. 251915.
(10) Das, S.; Zhang, W.; Demarteau, M.; Hoffmann, A.; Dubey, M.; Roelofs, A. Tunable Transport Gap in Phosphorene. Nano Lett. 2014, 14, 5733−5739.
(11) Peng, X.; Wei, Q.; Copple, A. Strain-Engineered Direct-Indirect Band Gap Transition and Its Mechanism in Two-Dimensional Phosphorene. Phys. Rev. B 2014, 90, No. 085402.
(12) Liu, H.; Neal, A. T.; Zhu, Z.; Luo, Z.; Xu, X.; Tománek, D.; Ye, P. D. Phosphorene: An Unexplored 2D Semiconductor with a High Hole Mobility. ACS Nano 2014, 8, 4033−4041.
(13) Castellanos-Gomez, A.; Vicarelli, L.; Prada, E.; Island, J. O.; Narasimha-Acharya, K. L.; Blanter, S. I.; Groenendijk, D. J.; Buscema, M.; Steele, G. A.; Alvarez, J. V.; et al. Isolation and Characterization of Few-Layer Black Phosphorus. 2D Mater. 2014, 1, No. 025001.
(14) Brent, J. R.; Savjani, N.; Lewis, E. A.; Haigh, S. J.; Lewis, D. J.; O'Brien, P. Production of Few-Layer Phosphorene by Liquid Exfoliation of Black Phosphorus. Chem. Commun. 2014, 50, 13338− 13341.
(15) Wood, J. D.; Wells, S. A.; Jariwala, D.; Chen, K.; Cho, E.; Sangwan, V. K.; Liu, X.; Lauhon, L. J.; Marks, T. J.; Hersam, M. C. Effective Passivation of Exfoliated Black Phosphorus Transistors against Ambient Degradation. Nano Lett. 2014, 14, 6964−6970.
(16) Wang, G.; Slough, W. J.; Pandey, R.; Karna, S. P. Degradation of Phosphorene in Air: Understanding at Atomic Level. 2D Mater. 2016, 3, No. 025011.
(17) Plutnar, J.; Sofer, Z.; Pumera, M. Products of Degradation of Black Phosphorus in Protic Solvents. ACS Nano 2018, 12, 8390− 8396.
(18) Zhou, Q.; Chen, Q.; Tong, Y.; Wang, J. Light-Induced Ambient Degradation of Few-Layer Black Phosphorus: Mechanism and Protection. Angew. Chem., Int. Ed. 2016, 55, 11437−11441.
(19) Huang, Y.; Qiao, J.; He, K.; Bliznakov, S.; Sutter, E.; Chen, X.; Luo, D.; Meng, F.; Su, D.; Decker, J.; et al. Interaction of Black Phosphorus with Oxygen and Water. Chem. Mater. 2016, 28, 8330− 8339.
(20) Kuntz, K. L.; Wells, R. A.; Hu, J.; Yang, T.; Dong, B.; Guo, H.; Woomer, A. H.; Druffel, D. L.; Alabanza, A.; Tománek, D.; et al. Control of Surface and Edge Oxidation on Phosphorene. ACS Appl. Mater. Interfaces 2017, 9, 9126−9135.
(21) Wang, G.; Slough, W. J.; Pandey, R.; Karna, S. P. Degradation of Phosphorene in Air: Understanding at Atomic Level. 2D Mater. 2016, 3, No. 025011.
(22) Ziletti, A.; Carvalho, A.; Trevisanutto, P. E.; Campbell, D. K.; Coker, D. F.; Castro Neto, A. H. Phosphorene Oxides: Bandgap Engineering of Phosphorene by Oxidation. Phys. Rev. B: Condens. Matter Mater. Phys. 2015, 91,1−10.
(23) Gusmão, R.; Sofer, Z.; Pumera, M. Functional Protection of Exfoliated Black Phosphorus by Noncovalent Modification with Anthraquinone. ACS Nano 2018, 12, 5666−5673.
(24) Wang, L.; Sofer, Z.; Pumera, M. Voltammetry of Layered Black Phosphorus: Electrochemistry of Multilayer Phosphorene. ChemElec-troChem 2015, 2, 324−327.
(25) Bogdanowicz, R.; Fabiańska, A.; Golunski, L.; Sobaszek, M.; Gnyba, M.; Ryl, J.; Darowicki, K.; Ossowski, T.; Janssens, S. D. D.; Haenen, K.; et al. Influence of the Boron Doping Level on the Electrochemical Oxidation of the Azo Dyes at Si/BDD Thin Film Electrodes. Diamond Relat. Mater. 2013, 39,82−88.
(26) Ryl, J.; Burczyk, L.; Bogdanowicz, R.; Sobaszek, M.; Darowicki, K Study on Surface Termination of Boron-Doped Diamond Electrodes under Anodic Polarization in H2SO4 by Means of Dynamic Impedance Technique. Carbon 2016, 96, 1093−1105.

(27) Nidzworski, D.; Siuzdak, K.; Niedziałkowski, P.; Bogdanowicz, R.; Sobaszek, M.; Ryl, J.; Weiher, P.; Sawczak, M.; Wnuk, E. E.; Goddard, W. A.; et al. A Rapid-Response Ultrasensitive Biosensor for Influenza Virus Detection Using Antibody Modified Boron-Doped Diamond. Sci. Rep. 2017, 7, No. 15707.
(28) Guo, Z.; Zhang, H.; Lu, S.; Wang, Z.; Tang, S.; Shao, J.; Sun, Z.; Xie, H.; Wang, H.; Yu, X. F.; et al. From Black Phosphorus to Phosphorene: Basic Solvent Exfoliation, Evolution of Raman Scattering, and Applications to Ultrafast Photonics. Adv. Funct. Mater. 2015, 25, 6996−7002.
(29) Lu, J.; Wu, J.; Carvalho, A.; Ziletti, A.; Liu, H.; Tan, J.; Chen, Y.;CastroNeto, A. H.;Ö zyilmaz, B.; Sow, C. H. Bandgap Engineering of Phosphorene by Laser Oxidation toward Functional 2D Materials. ACS Nano 2015, 9, 10411−10421.
(30) Zhang, Y.; Wang, H.; Luo, Z.; Tan, H. T.; Li, B.; Sun, S.; Li, Z.; Zong, Y.; Xu, Z. J.; Yang, Y.; et al. An Air-Stable Densely Packed Phosphorene−Graphene Composite Toward Advanced Lithium Storage Properties. Adv. Energy Mater. 2016, 6, No. 1600453.
(31) Woomer, A. H.; Farnsworth, T. W.; Hu, J.; Wells, R. A.; Donley, C. L.; Warren, S. C. Phosphorene: Synthesis, Scale-up, and Quantitative Optical Spectroscopy. ACS Nano 2015, 9, 8869−8884.
(32) Favron, A.; Gaufrès, E.; Fossard, F.; Phaneuf-Laheureux, A. L.; Tang, N. Y. W.; Lévesque, P. L.; Loiseau, A.; Leonelli, R.; Francoeur, S.; Martel, R. Photooxidation and Quantum Confinement Effects in Exfoliated Black Phosphorus. Nat. Mater. 2015, 14, 826−832.
(33) Kumar, V.; Brent, J. R.; Shorie, M.; Kaur, H.; Chadha, G.; Thomas, A. G.; Lewis, E. A.; Rooney, A. P.; Nguyen, L.; Zhong, X. L.; et al. Nanostructured Aptamer-Functionalized Black Phosphorus Sensing Platform for Label-Free Detection of Myoglobin, a Cardiovascular Disease Biomarker. ACS Appl. Mater. Interfaces 2016, 8, 22860−22868.
(34) Favron, A.; Goudreault, F. A.; Gosselin, V.; Groulx, J.; Côté, M.; Leonelli, R.; Germain, J.-F.; Phaneuf-L'Heureux, A.-L.; Francoeur, S.; Martel, R. Second-Order Raman Scattering in Exfoliated Black Phosphorus. Nano Lett. 2018, 18, 1018−1027.
(35) He, Y.; Leïchlé, T. Fabrication of Lateral Porous Silicon Membranes for Planar Microfluidics by Means of Ion Implantation. Sens. Actuators, B 2017, 239, 628−634.
(36) Fei, R.; Yang, L. Lattice Vibrational Modes and Raman Scattering Spectra of Strained Phosphorene. Appl. Phys. Lett. 2014, 105, No. 083120.
(37) Yau, S.-L.; Moffat, T. P.; Bard, A. J.; Zhang, Z.; Lerner, M. M. STM of the (010) Surface of Orthorhombic Phosphorus. Chem. Phys. Lett. 1992, 198, 383−388.
(38) Kistanov, A. A.; Cai, Y.; Zhou, K.; Dmitriev, S. V.; Zhang, Y.-W. The Role of H2O and O2molecules and Phosphorus Vacancies in the Structure Instability of Phosphorene. 2D Mater. 2017, 4, No. 015010.
(39) Wang, G.; Pandey, R.; Karna, S. P. Physics and Chemistry of Oxidation of Two-Dimensional Nanomaterials by Molecular iley Interdiscip. Rev.: Comput. Mol. Sci. 2017, 7, No. e1280.
(40) Edmonds, M. T.; Tadich, A.; Carvalho, A.; Ziletti, A.; O'Donnell, K. M.; Koenig, S. P.; Coker, D. F.; Ozyilmaz, B.; Neto, A. H. C.; Fuhrer, M. S. Creating a Stable Oxide at the Surface of Black Phosphorus. ACS Appl. Mater. Interfaces 2015, 7, 14557−14562.
(41) Mondal, S.; Sangaranarayanan, M. V. Permselectivity and Thickness-Dependent Ion Transport Properties of Overoxidized Polyaniline: A Mechanistic Investigation. Phys. Chem. Chem. Phys. 2016, 18, 30705−30720.
(42) Gusmão, R.; Sofer, Z.; Bouša, D.; Pumera, M. Black Phosphorus Synthesis Path Strongly Influences Its Delamination, Chemical Properties and Electrochemical Performance. ACS Appl. Energy Mater. 2018, 1, 503−509.
(43) Woomer, A. H.; Farnsworth, T. W.; Hu, J.; Wells, R. A.; Donley, C. L.; Warren, S. C. Phosphorene: Synthesis, Scale-Up, and Quantitative Optical Spectroscopy. ACS Nano 2015, 9, 8869−8884.
(44) Hirschorn, B.; Orazem, M. E.; Tribollet, B.; Vivier, V.; Frateur, I.; Musiani, M. Determination of Effective Capacitance and Film Thickness from Constant-Phase-Element Parameters. Electrochim. Acta 2010, 55, 6218−6227.
(45) Wysocka, J.; Cieslik, M.; Krakowiak, S.; Ryl, J. Carboxylic Acids as Efficient Corrosion Inhibitors of Aluminium Alloys in Alkaline Media. Electrochim. Acta 2018, 289, 175−192.
(46) Wysocka, J.; Krakowiak, S.; Ryl, J. Evaluation of Citric Acid Corrosion Inhibition Efficiency and Passivation Kinetics for Aluminium Alloys in Alkaline Media by Means of Dynamic Impedance Monitoring. Electrochim. Acta 2017, 258, 1463−1475.
(47) Boukamp, B. Electrochemical Impedance Spectroscopy. In Nano-Electrocatalysis; MESA Research Institute for Nanotechnology: The Netherlands, 2008; pp 24−28.